Y. Cao, M. Wojnowski, and B. K. Lau, "Circularly polarized sub-THz antenna design for distributed deployment," in *Proc. 18th Europ. Conf. Antennas Propag. (EuCAP'2024)*, Glasgow, UK, Mar. 17-22, 2024.

Circularly Polarized Sub-THz Antenna Design for Distributed Deployment

Yuyan Cao[1], Maciej Wojnowski[2], Buon Kiong Lau[1]
[1] Department of Electrical and Information Technology, Lund University, Sweden, yuyan.cao@eit.lth.se
[2] Infineon Technologies AG, Neubiberg, Germany

***Abstract*—Sub-THz deployment is challenging due to high propagation losses, necessitating dense deployment. To reduce cost, RF signal can be distributed via plastic fiber to remote radio units to increase coverage area. In this paper, we propose an antenna-in-package concept for the single-layer substrate on low-cost embedded wafer level ball grid array (eWLB) packages. To suppress the distortion in the broadside pattern from the coplanar waveguide feed line, the circularly polarized patch antenna is surrounded by an integrated loop structure. The loop also enhances the antenna bandwidth by adding a second resonance. Simulation results show that the proposed antenna offers broadside coverage with the 10 dB impedance and 3 dB axial ratio bandwidths of 14.2% and 11.2% at 145 GHz, as well as realized gain of 7.8 dBi. The antenna shows good promise for array implementation on eWLB packages.**

***Index Terms*—circularly polarized antennas, antenna array, subTHz band, dense deployment.**

I. Introduction

One major trend in 6G research is sub-THz deployment, due to the push to have higher peak data rates than those offered by 5G New Radio and the availability of large spectrum resources in the sub-THz range [1]. Multi-Gbps links are needed to support various applications, such as fixed wireless access, wireless backhaul, data distribution in airplanes and offices, as well as augmented reality (AR) and virtual reality (VR) [1]. However, high propagation loss at sub-THz frequencies requires new strategies for system design, especially where the user equipment (UE) is mobile. This is because mobility implies random device orientation, possibility of blockage (e.g., from user body or other large objects) and continuous coverage requirement.

The radiostripe concept [2], originally devised for sub-6 GHz distributed massive MIMO deployment, can be utilized to meet the challenges of sub-THz communications in indoor scenarios. Following this concept, polymer microwave fibers (PMFs) are deployed to extend the coverage area of each digital unit (DU) by carrying the RF signals to regularly spaced remote units (RUs) along the fiber, each equipped with its own broadside antenna to provide overlapping local coverage (see Fig. 1). Moreover, to allow for random UE orientation in a low complexity system design, circularly polarized (CP) antenna is preferred.

The embedded wafer level ball grid array (eWLB) package [3], [4] offers low-cost implementation of the RUs, as well as low loss, high-resolution RDL, precise wafer-level processing with low tolerances. However, its conventional single-layer substrate (mold layer) presents some limitations on antenna-in-package (AiP) realizations, relative to multi-layer substrates typical in more complex technologies such as low-temperature co-fired ceramics (LTCC) [1], PCB laminates [5], and liquid crystal polymer (LCP) [6].

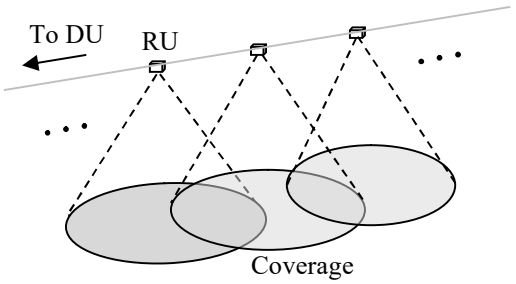

Fig. 1. A linear PMF with RUs for extended sub-THz coverage.

In this paper, we propose a D-band CP patch antenna suitable for array integration in an eWLB package. To keep the structure simple, the antenna and its feeding network are printed on the signal distribution layer, with the PCB connected to the eWLB package acting as a reflector. It was observed that the broadside pattern of a patch monopole antenna can be distorted by the coplanar waveguide (CPW) feed [7]. Characteristic mode analysis (CMA) [8] revealed that the pattern distortion is due to an unwanted mode introduced by the feed structure. To mitigate this effect, the patch monopole radiator is encircled by a loop. However, the loop also introduces a new degenerate mode, which can be tuned by adding slots on the edges of the patch to enable dual resonance. Finally, the loop-patch antenna is implemented on an eWLB-like substrate with a finite PCB ground. Circular polarization is enabled by corner truncation of the patch (and corresponding reshaping of the loop) to concurrently excite the degenerate modes of the patch and the loop at their resonances. Several elements of the proposed antenna can be used to form an array to achieve higher gain and spatial selectivity for application in an RU.

II. Coplanar Antenna and Feed Design

For the specific eWLB AiP implementation considered in this work, the antenna should be printed on the bottom side of a single-layer substrate, with an air layer and a reflector at the bottom (see Fig. 2). The substrate primarily has a loading effect and slightly affects the antenna's main

978-88-31299-09-1/24/$31.00 ©2024 IEEE

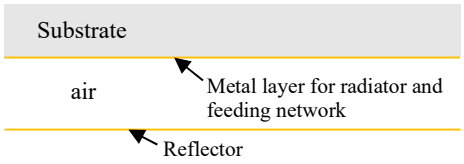

Fig. 2. Single-layer substrate with metal layer, air gap and reflector.

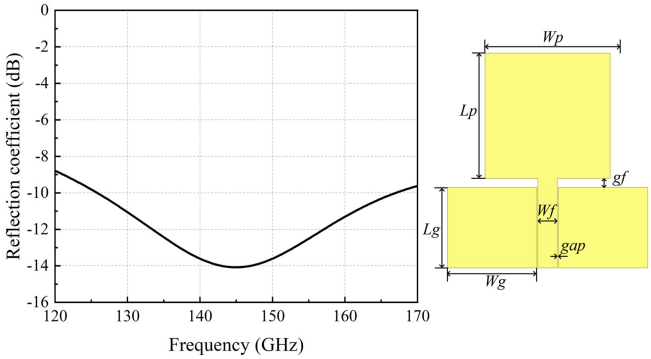

Fig. 3. Reflection coefficient of square monopole patch antenna with CPW feed line and reflector (below). Antenna and reflector simulated with 12μm and 35μm thin perfect electric conductors (PECs), respectively, Infinite and 3 × 3 mm^2 reflector sizes used for the CMA and full-wave simulations, respectively. (Wp = 0.84, Lp = 0.84, Wg = 0.6, Lg = 0.53, Wf = 0.135, gap = 0.01, gf = 0.07. Unit: mm)

operating principles, thus it was first ignored to ease CMA. CMA and full-wave simulations were run in the method-of-moments solver of 2022 Altair FEKO and the finite-element method solver of 2023 Ansys HFSS, respectively.

A. Conventional Square Patch with Reflector

The lowest order characteristic modes (CMs) of a square metal patch are two degenerate modes, i.e., the fundamental (half-wave) dipole modes along the patch's two dimensions with orthogonally polarized far-field patterns [9]. Therefore, a reflector placed a quarter-wavelength below the patch will result in a simple broadside antenna solution, capable of offering the broadside coverage shown in Fig. 1.

However, due to the use of only one metal layer, CPW is used to realize a 50Ω feed line. A common feed placement to excite one of the dipole modes is shown in Fig. 3, forming what is commonly known as a wideband monopole [10]. For this simple structure, fed by a wave port in Ansys HFSS, the 10 dB impedance bandwidth is 28% at the center frequency of 145 GHz. However, this arrangement (with Wg = 0.6 mm) not only excites the dipole mode of interest (Mode 1 in Figs. 4 and 5, with current along the feedline direction), but also a new mode (i.e., Mode 2 in Figs. 4 and 5) created by the CPW feed structure. For the CMA, two wire ports are located at the bottom end of the CPW line to excite the structure. The new mode causes a slight tilt in the broadside pattern (see Fig. 6(a)). The beam tilt mainly results from the constructive and destructive interference of the two modal far-field patterns (depicted in Fig. 4) due to their respective phase distributions [11]. For implementation on eWLB packages, a narrow ground is preferred for the CPW feed line. However, the narrower CPW line structure

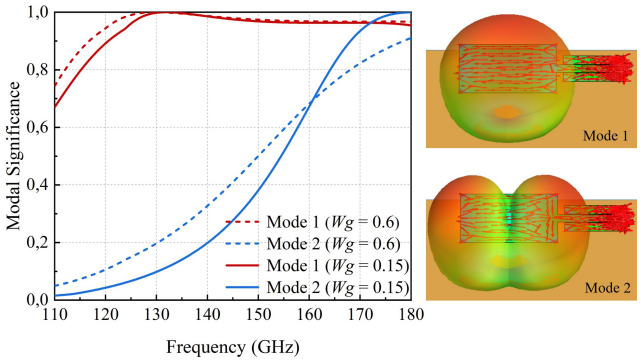

Fig. 4. Modal significance and far-field patterns/currents of the patch monopole antenna in Fig. 3 of two modes of interest for two different Wg.

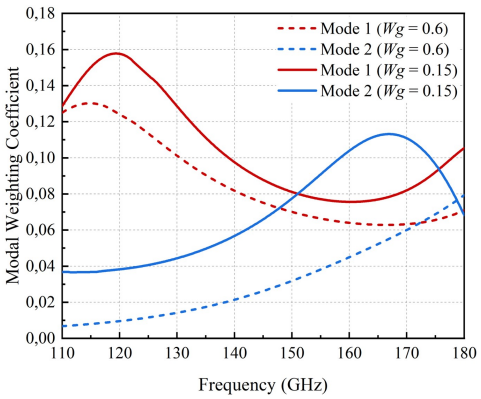

Fig. 5. Modal weighting coefficient in Fig. 3 of two modes of interest for two different Wg's.

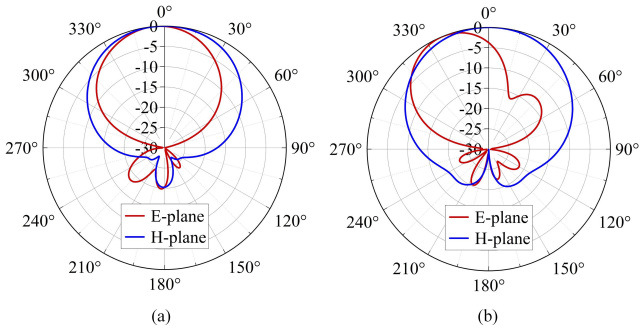

Fig. 6. Normalized realized gain pattern (in dB) of the antenna at 145 GHz with (a) Wg = 0.6 and (b) Wg = 0.15. (Unit: mm)

leads to a larger beam tilt (see Fig. 6(b)). This is because a smaller Wg causes Mode 2's resonant frequency to decrease, resulting in Mode 2 contributing more to the radiation in the band of interest, as can be seen in Figs. 4 and 5.

B. Square Patch with Outer Loop and Reflector

To mitigate the contribution of the CPW feed line to the antenna pattern, a ground-integrated outer loop is added to the square patch (see Fig. 7), to provide the patch radiator with more uniform coupling to the CPW ground. With this addition, the unwanted mode (Mode 2) is no longer excited significantly. Similar outer loop structures were proposed for D-band patch antenna (see e.g., [3]), but not to address the beam tilting problem.

The CMA of this new loop-patch structure revealed that the unwanted mode due to the CPW line was no longer

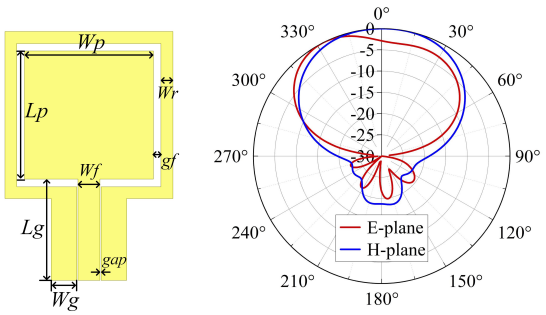

Fig. 7. Square patch (with outer loop) and reflector (below) simulated with 12μm and 35μm thin PECs, respectively, and its normalized far-field pattern (in dB). Infinite and 3 × 3 mm^2 reflector sizes used for the CMA and full-wave simulations, respectively. (Wp = 0.76, Lp = 0.76, Wg = 0.15, Lg = 0.6, Wf = 0.13, gap = 0.007, gf = 0.045, Wr = 0.07. Unit: mm)

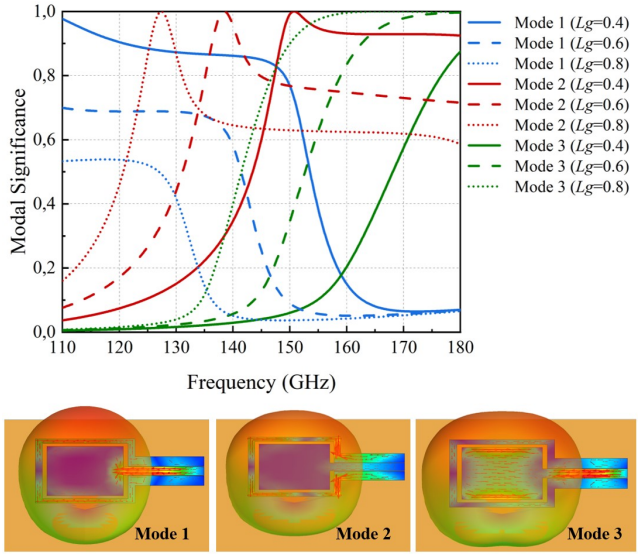

Fig. 8. Modal significance and far-field patterns/currents of three broadside modes of loop-patch antenna.

significant in the frequency range of interest. As shown in Fig. 8, the overall loop-patch structure yields three resonant (broadside) modes of interest in the D-band, with Modes 1-3 contributed mainly by the currents in the loop-CPW structure, the loop structure and the patch structure, respectively. However, the length of the CPW line (Lg) has a dominant effect on all three modes. As can be seen in Fig. 8, an increase in Lg leads to lower modal resonant frequencies for Modes 1-3. In this work, Modes 2 and 3 are utilized to achieve a dual-resonance wideband monopole patch antenna, considering their broadside pattern as well as the presence of corresponding (cross-polarized) degenerate modes that will later enable dual-resonance CP operation. By tuning the resonances, the antenna yields a (single-polarized) dual-resonance 10 dB impedance bandwidth of 19.2% (130.8-158.7 GHz) and the peak realized gain is ~6 dBi (see Fig. 9). The in-band total efficiency is ≥ 90% (–0.46 dB) due to lossless PEC and ≥ 10 dB return loss.

C. Slotted Square Patch with Outer Loop and Reflector

To further increase the flexibility in tuning the dual resonances, slots can be etched into the two radiating edges

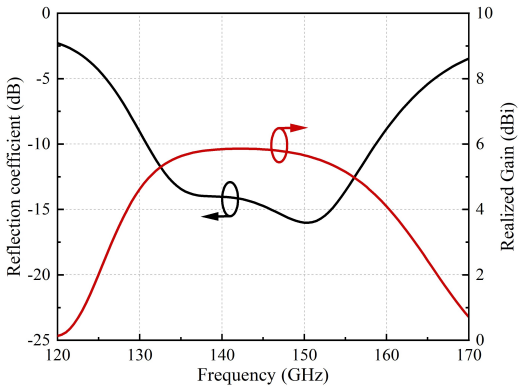

Fig. 9. Reflection coefficient and realized gain of loop-patch antenna.

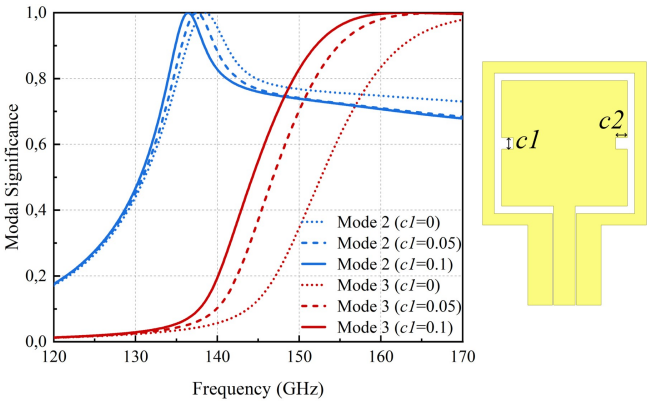

Fig. 10. Modal significance of the loop (Mode 2) and patch (Mode 3) with different slot lengths. Loop-patch structure with two slots etched on the patch shown to the right.

of the patch mode (see the right subplot of Fig. 10). As expected, the slots induce a larger shift in the patch mode (Mode 3) than the loop mode (Mode 2), as shown in Fig. 10.

III. Practical Implementation on Substrate

For proof of concept, an Astra MT77 substrate (thickness of 0.4445 mm, permittivity of 2.8 and loss tangent of 0.0058 [12]) was used for the antenna design using the FEM solver of 2023 Ansys HFSS. The parameter values are similar to the physical and electrical properties of eWLB substrates, which facilitates validation of antenna concepts for eWLB. The dimensions of the no-substrate single-polarized antenna presented in Section II-B were adjusted accordingly for the substrate properties and the distance to the ground is decreased according to eWLB implementation. As can be expected, the impedance bandwidth decreases slightly with the dielectric substrate.

To achieve circular polarization, the standard technique of truncating a pair of diagonally opposite corners of the patch was adopted. The loop was also reshaped around the truncated corners. Furthermore, to enhance and align the impedance bandwidth and axial ratio (AR) bandwidth, the patch and the loop dimensions were optimized to tune the degenerate patch and loop modes' resonances. The resulting design is presented in Fig. 11.

In this design, the patch is printed on the bottom side of the substrate (see Fig. 2). As explained in Section II-C, the

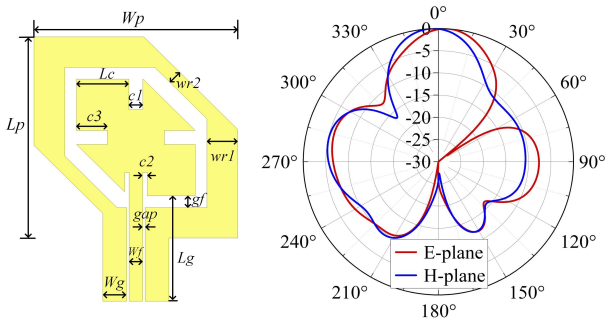

Fig. 11. Truncated square patch with outer loop with 3.6 × 3.85 mm^2 reflector (0.244 mm below the substrate), and its normalized far-field pattern (in dB). Antenna and reflector simulated with 12μm and 35μm thin copper layers, respectively. (*Wp* = 0.86, *Lp* = 0.86, *Wg* = 0.1, *Lg* = 0.45, *Lc* = 0.22, *Wf* = 0.056, *gap* =0.011, *gf* = 0.05, *Wr1* = 0.13, *Wr2* = 0.06, *c1* = 0.06, *c2* = 0.02, *c3* = 0.13. Unit: mm)

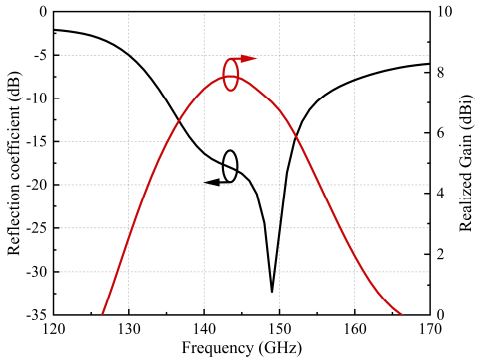

Fig. 12. Reflection coefficient and realized gain of the truncated square patch with outer loop and finite reflector.

resonant frequencies of the loop and patch are brought closer to each other by etching the slots on the patch, though here the slots are added on all four sides due to CP operation. The unwanted modes were moved out of the band of interest by adjusting the length of the feed line, facilitating the broadside pattern shown in Fig. 11. In addition, the size of the reflector and the distance between the reflector and the substrate were optimized to 3.6 mm × 3.85 mm and 0.244 mm, respectively, to further increase the gain. Furthermore, the relatively thick dielectric substrate (here functioning as a superstrate) serves as a lens, enhancing the antenna gain but at the cost of increased side lobe level. The final simulated results are shown in Figs. 12 and 13: the 10 dB impedance bandwidth is 14.2% (134.8-155.5 GHz), the maximum realized gain is 7.8 dBi, the peak total efficiency is 89% (–0.5 dB) and the 3 dB AR bandwidth is 11.2% (136.2-152.4 GHz).

IV. Conclusions

This work presents the design of a D-band AiP concept for eWLB packages based on a CPW-fed CP patch antenna with a reflector. Appropriate design of the CPW feed line helps to mitigate its effect on the desired broadside pattern. Furthermore, the impedance and AR bandwidths are enhanced by adding a loop structure around the patch, yielding 14% and 11% bandwidths, respectively. Possible future work includes experimental validation as well as extension to array implementation.

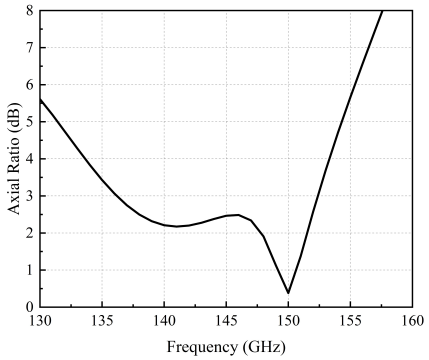

Fig. 13. Axial ratio of the truncated square patch with outer loop and finite reflector.

Acknowledgment

This work is supported by the Horizon Europe (HEU) project 6GTandem.

References

[1] T. Maiwald, et al.,"A review of integrated systems and components for 6G wireless communication in the D-Band," *Proc. IEEE*, vol. 111, no. 3, pp. 220-256, Mar. 2023.

[2] E. Ernforns. (2019) Radio stripes: re-thinking mobile networks. [Online]. Available: https://www.ericsson.com/en/blog/2019/2/radio-stripes

[3] A. Bhutani, E. Bekker, L. G. de Oliveira, M. Pauli, and T. Zwick, "140 GHz broadband antenna in embedded wafer-level ball grid array technology," in *Proc. 15th Europ. Conf. Antennas Propag. (EuCAP 2021)*, Dusseldorf, Germany, 2021, pp. 1-5.

[4] I. Nasr *et al*., "A highly integrated 60 GHz 6-channel transceiver with antenna in package for smart sensing and short-range communications," *IEEE J. Solid-State Circuits*, vol. 51, no. 9, pp. 2066-2076, Sep. 2016.

[5] A. Lamminen, J. Säily, J. Ala-Laurinaho, J. de Cos, and V. Ermolov, "Patch antenna and antenna array on multilayer high-frequency PCB for D-band," *IEEE Open J. Antennas Propag*., vol. 1, pp. 396-403, 2020.

[6] B. Zhang, C. Kärnfelt, H. Gulan, T. Zwick and H. Zirath, "A D-band packaged antenna on organic substrate with high fault tolerance for mass production," *IEEE Trans. Comp. Pac. Man. Tech*., vol. 6, no. 3, pp. 359-365, Mar. 2016.

[7] A. K. Gautam, S. Yadav and B. K. Kanaujia, "A CPW-fed compact UWB microstrip antenna," *IEEE Antennas Wireless Propag. Lett.*, vol. 12, pp. 151-154, 2013.

[8] R. Harrington and J. Mautz, "Theory of characteristic modes for conducting bodies," *IEEE Trans. Antennas Propag.*, vol. 19, no. 5, pp. 622-628, Sep. 1971.

[9] D. Manteuffel and R. Martens, "Compact multimode multielement Antenna for Indoor UWB Massive MIMO," *IEEE Trans. Antennas Propag*., vol. 64, no. 7, pp. 2689-2697, Jul. 2016.

[10] E. Antonino-Daviu, M. Cabedo-Fabres, M. Ferrando-Bataller, A. Valero-Nogueira, "Wideband double-fed planar monopole antennas, " Electron. Lett., vol. 39, no. 23, pp. 1635-1636, Nov. 2003.

[11] X. Fu, Z. Zhang, and J. Wang, "A compact frequency scanning planar array using characteristic mode analysis," *IEEE Antennas Wireless Propag. Lett.*, vol. 20, no. 9, pp. 1666-1670, Sep. 2021.

[12] A. Kanitkar, I. Ndip, M. Chernobryvko, J. M. Köszegi, O. Schwanitz and M. Schneider-Ramelow, "A comparative analysis of two dielectric extraction methods of a PCB material for D-Band applications," in *Proc. 2022 IEEE 9th Electron. Syst.-Integr. Technol. Conf. (ESTC 2022)*, Sibiu, Romania, 2022, pp. 350-353.